

DOI: 10.1002/adfm.200701001

# Synthesis of Thin, Oriented Zeolite A Membranes on a Macroporous Support\*\*

By Tatsiana A. Kuzniatsova, Matthew L. Mottern, William V. Chiu, Yanghee Kim, Prabir K. Dutta, and Henk Verweij\*

Continuous, thin, oriented zeolite A membranes are produced by a two-step synthesis on macroporous  $\alpha$ -Al<sub>2</sub>O<sub>3</sub> supports. In the *first step*, zeolite A nano-cubes with ~350-nm edges are prepared as a native impurity phase in zeolite Y synthesis dispersions, the support surface is pre-modified with a cationic polymer having a selective affinity for zeolite A. The thus-treated support is contacted with a colloiddally stable dispersion of zeolite A and Y mixture in water, which results in selective, dense-packed deposition of the zeolite A cubes with one face aligned to the average support surface. In a *second step* of hydrothermal epitaxial growth, the seed layer grows epitaxially into a continuous, meso-defect free, ~1  $\mu$ m thick zeolite A layer, already after 1 h of treatment. This microstructure of the membrane compares very favorably to what is commonly obtained. The pH value of the zeolite mixture suspension is found to have a major influence on seed layer morphology, and thereby, on the quality and orientation of zeolite A membrane after short synthesis times. The final zeolite A membrane thickness and morphology is controlled by varying secondary growth synthesis time. The approach presented is thought to be of generic use for the preparation of oriented zeolite membranes.

## 1. Introduction

Zeolite thin films and layers are of great interest for use as membranes in separation devices and membrane reactors,<sup>[1–6]</sup> chemical sensors,<sup>[7]</sup> and hosts for guest species.<sup>[8]</sup> These species can add important chemical, optical, electrical and/or magnetic properties.<sup>[7]</sup> Although oriented zeolite structures are of interest for all these applications, their viable and reproducible synthesis is still a challenge, in particular on porous substrates.

Oriented zeolite films have been synthesized on dense supports by *in situ* growth, but two-step synthesis methods are generally found to give better results.<sup>[9]</sup> In two-step synthesis, an oriented seed layer is deposited on the support surface, followed by epitaxial formation of a continuous structure in which the original seed layer orientation is preserved.<sup>[9]</sup> The significant differences between the nature and mechanisms of the subsequent steps make that the best result is obtained with a separate optimization of the conditions for each step.<sup>[10]</sup>

Several groups have reported on the development of oriented zeolite membranes with the thicknesses of 3–10  $\mu$ m

through a two-step synthesis on smooth nonporous supports which include silicon wafers,<sup>[7,9,11,12]</sup> single-crystal<sup>[11]</sup> and polished<sup>[13]</sup> quartz, glass,<sup>[9,14]</sup> metal films,<sup>[7]</sup> non-graded,<sup>[10]</sup> poly-crystalline,<sup>[15]</sup> or single-crystal<sup>[16]</sup> alumina. Macroporous supports are applied to provide strength to the membrane, and at the same time, sufficient permeability for species that are separated by the membrane. State of the art macroporous supports, however, have a surface porosity and related roughness that tend to randomize any seed crystal orientation. To avoid this effect, a ~2  $\mu$ m thick mesoporous silica buffer layer was applied<sup>[17–19]</sup> to mask the porosity and diminish roughness. The application of such layers, however, may decrease thermo-chemical stability of the structure because of unavoidable (dynamic) thermal mismatches between the support and the buffer layer. In addition, very thick mesoporous layers may increase the overall gas transport resistance.<sup>[10,20]</sup>

To our knowledge, there are no examples of successful synthesis of oriented zeolite A membranes directly on native macroporous supports. In this work, we demonstrate how continuous, oriented membranes of zeolite Na–A can be made on smooth macroporous supports by selective sorption of seed crystals, mixed with inert particles, followed by epitaxial secondary growth.

## 2. Results and Discussion

### 2.1. Zeta Potential Measurements and Zeolite A Seed Layer Formation

A negative surface charge is reported for zeolite powders and  $\alpha$ -Al<sub>2</sub>O<sub>3</sub> in basic media<sup>[9,21]</sup> so that electrostatic double layer repulsion inhibits the adsorption of zeolite particles (in particular A) onto the  $\alpha$ -Al<sub>2</sub>O<sub>3</sub> substrate. And vice versa, a

[\*] Prof. H. Verweij, Dr. T. A. Kuzniatsova, Dr. M. L. Mottern, W. V. Chiu  
Department of Materials Science & Engineering,  
Ohio State University  
2041 College Road, Columbus, OH 43210 (USA)  
E-mail: verweij.1@osu.edu

Dr. Y. Kim, Prof. P. K. Dutta  
Department of Chemistry, Ohio State University  
120 W 18th Avenue, Columbus, OH 43210 (USA)

[\*\*] This work is supported by the Basic Research for the Hydrogen Fuel Initiative Program (DOI, grant No. DF-FG01-04FR04-20). The authors also thank K. Shqau for Figure 3e and f accordance, as well as M. Schillo for FIB assistance.

positive support surface is expected to promote zeolite particle sorption.<sup>[21]</sup> Therefore, a zeolite A seed layer was prepared by surface modification of the support with a cationic polymer, poly(diallyldimethylammonium chloride) (PDDA),<sup>[22–25]</sup> followed by selective adsorption from a suspension mixture of negatively charged zeolite A and Y particles at optimized pH.

The supports were first immersed in the modification solution containing PDDA. The presence of a PDDA layer was confirmed by the appearance of dark areas on the  $\alpha$ -Al<sub>2</sub>O<sub>3</sub> surface due to carbon formation by polymer pyrolysis in the scanning electron microscopy (SEM) beam (Fig. 1). The support macro-pores were still clearly visible in the SEM image after polymer modification, indicating that the PDDA layer acts primarily as a surface-charge modifier, and does not smoothen the deposition surface.

A crystal mixture of zeolite Y and 1 vol % A was used for the seed layer adsorption step.<sup>[26]</sup> The pH at which optimal dispersion occurs was found from electro-acoustic measurements of the zeolite A and Y zeta potential ( $\zeta$ ). The initial assumption was that a significant negative zeolite surface charge density, and a large difference of this value between A- and Y-crystals are both required to prevent agglomeration, maintain suspension stability, and supply sufficient selectivity in seed layer sorption.

Indeed, sorption experiments at pH 8.5 ( $\zeta = -44$  and  $-17$  mV for zeolite A and Y, respectively, (Fig. 2)) showed the deposition of a thick, rough and randomly oriented layer of both A- and Y-particles (Fig. 3a) while at pH 11.7, a monolayer of pure, densely arranged zeolite A crystals was produced already after one adsorption cycle (Figs. 3b, c, and 4, curve a). At pH 11.7,  $\zeta$  of zeolite A was found to be  $-250$  mV, and Y had a much smaller value of  $-63$  mV (Fig. 2). Evidently, the zeolite A and Y surface charges at pH 11.7 are sufficient to maintain overall dispersion stability while the difference in  $\zeta$  of  $>180$  mV results in near-complete selectivity for the sorption of the zeolite A minority phase onto the positively modified  $\alpha$ -Al<sub>2</sub>O<sub>3</sub> surface, see Figure 5.

It is postulated that the mixture of weakly charged majority phase (zeolite Y) and strongly charged minority phase (zeolite A) is thought to be essential for the formation of dense-packed,

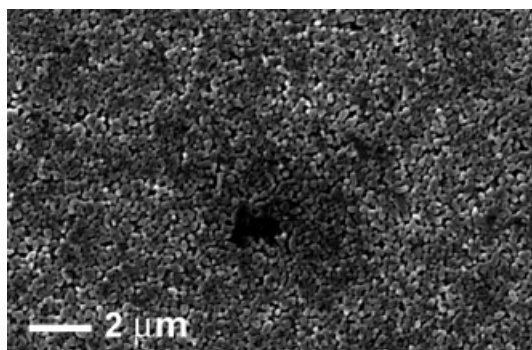


**Figure 1.** SEM image of an  $\alpha$ -Al<sub>2</sub>O<sub>3</sub> support after surface modification by PDDA. The dark area in the center is caused by carbon, formed by pyrolysis of PDDA in the 15 kV electron beam.

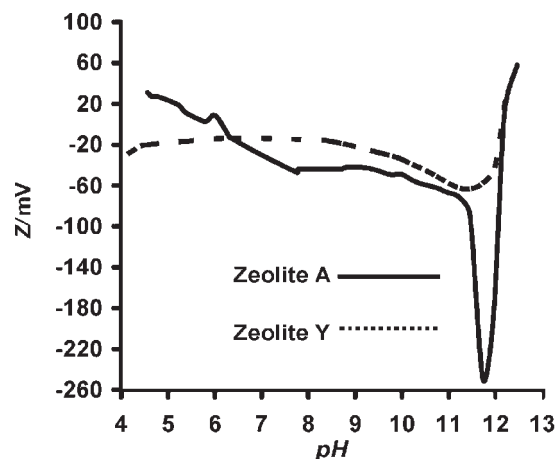


**Figure 2.** Zeta potential vs. pH for zeolite A and Y crystals in aqueous suspension.

near-perfect zeolite A depositions as shown. The inert Y-particles slow down deposition so that the A-particles have sufficient time to settle, which is comparable to the situation of slow growth of highly-perfect crystals at low super-saturation. At the same time, the deposition of additional zeolite particles on a thus-formed monolayer is hindered by the strong negative double layer repulsion between the monolayer and the dispersed crystals.

The seed layer thickness provides the ultimate lower limit for the thickness that can be obtained for a continuous membrane by secondary growth.<sup>[10]</sup> Therefore, the  $\sim 350$  nm dimensions of the individual A-crystals in the monolayer offer promise for major reductions in membrane thickness. Moreover, the excellent support smoothness (Fig. 3d–f) and the clear cube morphology of the zeolite A particles is found to result in a high degree of preferential [200] orientation after the deposition (Fig. 4, curve a). The charge-assisted sorption process shown, leads to a high degree of substrate coverage, and a well-adhering layer. We found that it was necessary to apply a heat treatment to improve adhesion before secondary hydrothermal step.<sup>[27]</sup> The excellent adhesion strength, right after deposition, was derived from the fact that the coverage remained non-defective after vigorous washing with water.

The FIB-TEM image (Fig. 3c) clearly indicates that there are no zeolite particles inside the substrate pores. The substrate pore had a typical diameter ( $\varnothing_p$ ) of  $\sim 40$  nm and can be considered as the interstitial space between three dense-packed surface grains of  $\alpha$ -Al<sub>2</sub>O<sub>3</sub>; these grains were  $<300$  nm in size, smaller than the bulk ones.<sup>[28]</sup> This was also confirmed by energy dispersive X-ray spectrometry (EDX) analysis of the cross-section shown, which did not reveal any silicon in the support (Fig. 6). The very fine particles seen in Figure 3c between the support and cubic zeolite A are smaller A-crystals, which was confirmed by EDX and microscopic particle shape investigations. They are formed in the synthesis of the primary zeolite particle mixture; their number concentration is likely higher than that of the  $\sim 350$  nm cubes.

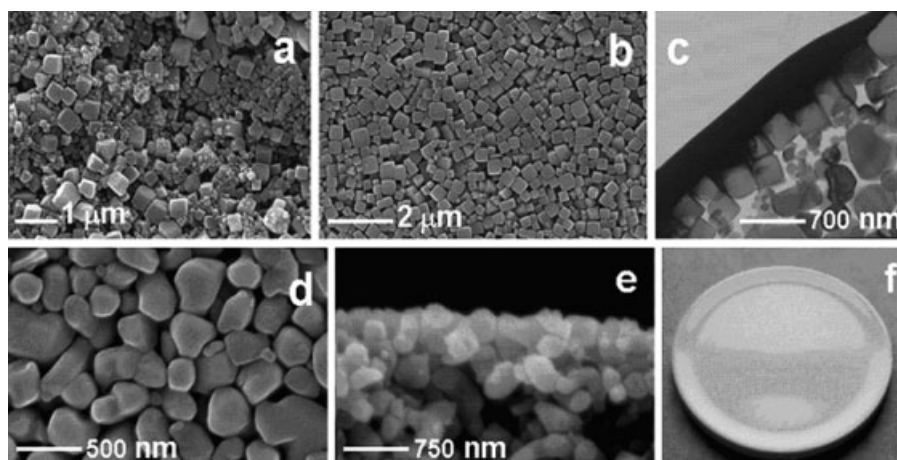


**Figure 3.** a) SEM surface view of  $\alpha$ - $\text{Al}_2\text{O}_3$  support seeded with zeolite crystals at pH 8.5. The large cubic crystals are zeolite A; the smaller (pyramidal) crystals are zeolite Y. b) Surface SEM, and c) transmission electron microscopy (TEM) image of a focused ion beam (FIB) cross-section of the support, seeded with zeolite A crystals at pH 11.7. The dark upper area in c) is a Pt layer, applied during FIB sample preparation. d) Surface and e) cross-section SEM of uncovered support; f) life-sized image showing support optical smoothness.

Contrary to what is the case for dense substrates,<sup>[29,30]</sup> dense-packed oriented zeolite monolayers were not realized on large macroporous areas before. Complete monolayer coverage by adsorbed zeolite A crystals was reproducibly obtained in this work for macroporous  $\alpha$ - $\text{Al}_2\text{O}_3$  in all depositions at pH 11.7 with only one coating treatment from the zeolite mixture. The above-presented deposition method is thought to be of generic use for the preparation of continuous, thin, oriented zeolite membranes.

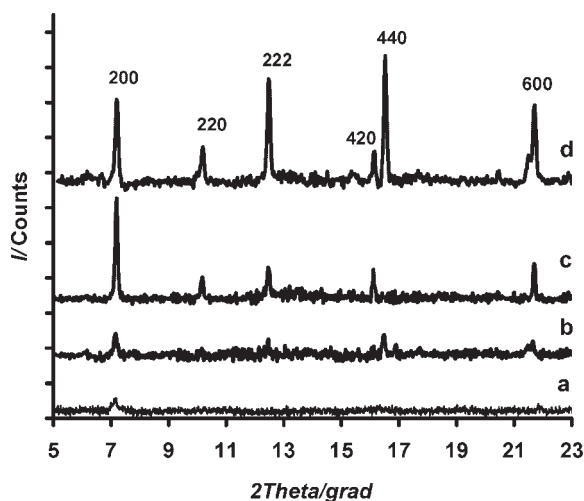


**Figure 4.** XRD spectra of a) [200]-oriented zeolite A seeds on the  $\alpha$ - $\text{Al}_2\text{O}_3$  support (shown in Fig. 3b and c), as well as zeolite A membrane after b) 1, c) 2, and d) 8 h of secondary growth. Comparison of the [200], [220], and [222] intensities shows that the relative growth rates for zeolite A depend on the crystallographic orientation, and that the fastest growth direction is [222] for the temperature and solution concentration used. This observation is consistent with the formation of A-cubes, bound by slowly growing [200] grains during crystal synthesis; the same mechanism, however, leads to eventual randomization of an initially oriented membrane.

## 2.2. Zeolite A Membrane Secondary Growth

The closely packed, oriented precursor layers were hydrothermally treated in a homogenous synthesis solution at 80 °C to prepare continuous, intergrown membranes. Secondary growth proceeds initially by local epitaxy on the deposited particles.<sup>[9]</sup> Later in the process, new, randomly oriented zeolite nuclei start to form.<sup>[9,13,15,18]</sup> Indeed, during a short growth time (1 h), the membrane maintained the predominant [200] orientation (Fig. 4, curve b). The film had in that case a thickness of  $\sim 1 \mu\text{m}$ , showed good adhesion to the support, and inspection by SEM did not reveal any micro-crack formation. The synthesis time to obtain a continuous layer was much less

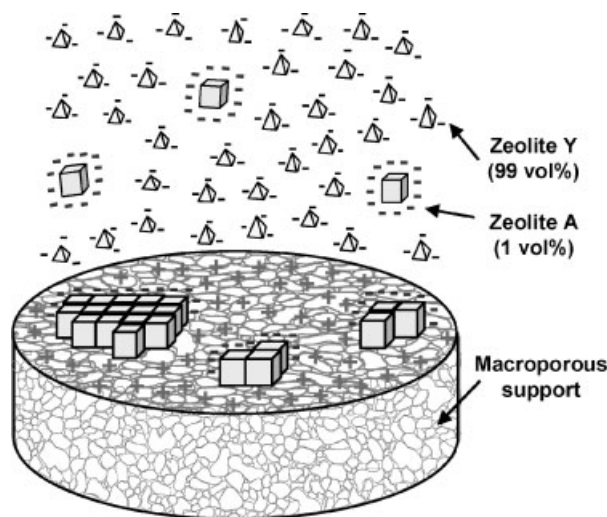


**Figure 5.** Selective adsorption of strongly negatively charged zeolite A crystals from mixed (A+Y)-suspension on the positively charged macroporous  $\alpha$ - $\text{Al}_2\text{O}_3$  support at pH 11.7. Dimensions are not to scale; the zeolite A concentration is exaggerated. The compensating cations are  $\text{TMA}^+$ , and the ionic strength is  $\sim 0.005$ .

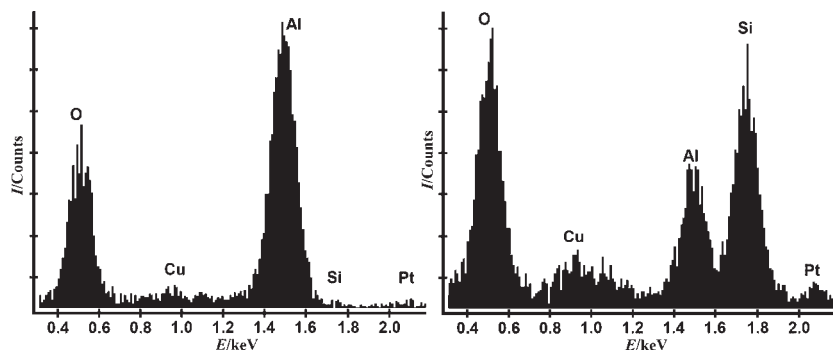


**Figure 6.** EDX spectra of: a)  $\alpha$ - $\text{Al}_2\text{O}_3$  support, and b) the zeolite A layer taken from the sample shown in Figure 3c (without removal of the zeolite A layer from the support). The copper peaks are caused by the TEM grid.

than what is needed for secondary growth of less ordered, nonclose-packed precursor layers.<sup>[9]</sup>

We like to emphasize that the quality of the diffractograms obtained for the thinnest membranes (Fig. 4) is sufficient to make conclusive statements about orientational changes during the crystallization process. The low-intensity [600] peak is clearly present while other, more intense, powder diffraction peaks of zeolite A are not at all present in the spectra (cf. with<sup>[31]</sup>).

After 2 h treatment, the layer thickness was on average 2  $\mu\text{m}$  and still fairly uniform throughout the membrane surface (Fig. 7a). The zeolite A remained highly (80%) [200]-oriented (Fig. 4, curve c), as was derived from the XRD intensity ratio  $I(200)/I(220)=6.0$  for the (200) and (220) peaks of the membrane, as opposed to 1.2 for randomly oriented zeolite A.<sup>[31]</sup> Although slightly misoriented, this membrane did not show any solution-nucleated crystals attached to its surface (Fig. 7a). This provides evidence for two different mechanisms for the formation of new nuclei during hydrothermal treatment: a) surface nucleation (obviously, takes place at short synthesis times), and b) solution nucleation (appears at longer times). Also, SEM cross-section images did not reveal any zeolite growth in the support pores. Such “support invasion” is known to increase the amount of defects and/or reduce the flux in zeolite membranes.<sup>[10]</sup>

Longer secondary treatments resulted in the appearance of a large population of newly formed grains in the growing film,

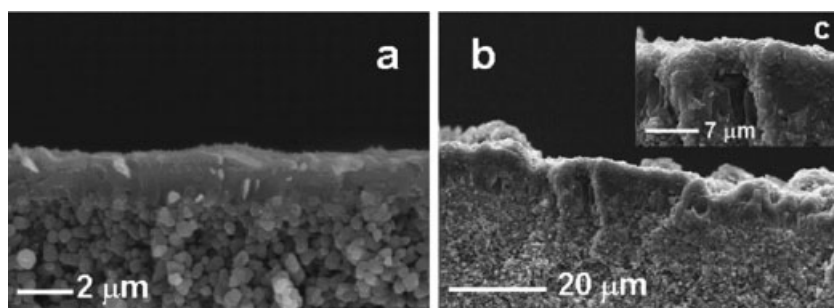


**Figure 7.** SEM cross-sectional view of zeolite A membrane after a) 2 and b), c) 21 h of secondary growth; b) view at low and c) at high magnification.

which led to a completely misoriented zeolite layer already after 8 h of synthesis (Fig. 4d). For this case, the membrane thickness was estimated to be  $\sim 4.5$   $\mu\text{m}$  from SEM cross-sections. All XRD spectra (Fig. 4) showed pure, well-crystallized zeolite A after secondary growth. Significant narrowing of the membrane XRD peaks, compared to those of seed layer, was found already after 1 h, and especially after  $>2$  h of the treatment. This provides evidence that the seed crystals grow and develop into a continuous membrane by epitaxy. After 21 h of secondary growth, a  $\sim 10$   $\mu\text{m}$  thick membrane was formed (Fig. 7b and c). In

that case, misoriented crystals settled from the solution were clearly observed on top of secondary-grown membrane. For the sake of comparison, a zeolite A membrane was grown by the in situ method (without applying seeds) at the same conditions (support type, synthesis temperature and starting gel composition). This membrane had a thickness of only 2–3  $\mu\text{m}$  after 70 h of growth (Fig. 8). Both membranes showed a non-uniform thickness.

Altogether, the membrane formation studies revealed that suspension pH is an important factor, influencing the zeolite particle adsorption process for producing thin, smooth, continuous and oriented crystal seed layers. The zeolite seed layer morphology, in turn, strongly influences the secondary treatment results; the zeolite A orientation obtained in seed layer deposition is preserved during short secondary treatment times.

### 2.3. Membrane Selectivity and Gas Permeance

Since the presence of connected meso- and macro-defects in the membranes cannot be completely determined from electron microscopy results, two types of transport characterizations were undertaken. First, the zeolite A membrane, formed after 1 h of hydrothermal treatment, was used for steady-state single gas permeation measurements (SGP). He,  $\text{H}_2$ , and  $\text{N}_2$ , chosen for SGP, have kinetic diameters ( $\varnothing$ ) of 0.26, 0.29, and 0.37 nm, respectively. Because of low molecular weight, these gases are not expected to be strongly sorbed in the zeolite membranes and to block membrane mesopore defects by capillary condensation, especially at higher temperatures.

To remove water adsorbed by zeolite A surface, the membrane was evacuated at 100  $^\circ\text{C}$  for 12 h before each gas-transport experiment. SGP measurements (conducted at 170  $^\circ\text{C}$  with vacuum at the permeate side and up to  $2 \times 10^5$  Pa at the feed side) confirmed the formation of continuous zeolite A membranes after 1 h of hydro-

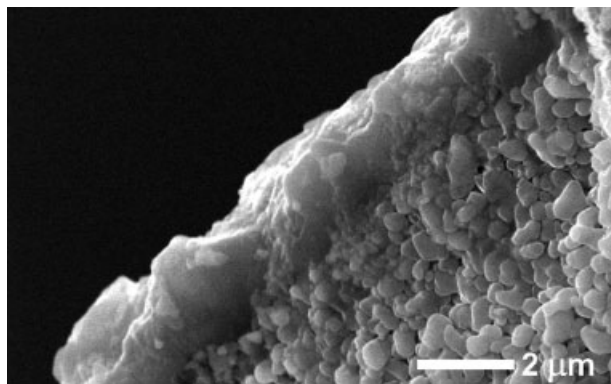


**Figure 8.** SEM cross-sectional view of a zeolite A membrane after 70 h of in situ growth (without applying seeds).

thermal treatment, establishing the presence of dominant microporous transport behavior. The membrane showed an overall He permeance of  $\sim 1 \times 10^{-7} \text{ mol m}^{-2} \text{ s}^{-1} \text{ Pa}^{-1}$  (much less than  $\sim 3 \times 10^{-6} \text{ mol m}^{-2} \text{ s}^{-1} \text{ Pa}^{-1}$  of the  $\alpha\text{-Al}_2\text{O}_3$  support).  $\text{H}_2/\text{N}_2$  permselectivity was  $\sim 4.80$  (permeances of  $\sim 2.16 \times 10^{-7}$  and  $\sim 4.5 \times 10^{-8} \text{ mol m}^{-2} \text{ s}^{-1} \text{ Pa}^{-1}$  for  $\text{H}_2$  and  $\text{N}_2$ , respectively), which is higher than the theoretical Knudsen selectivity value of 3.74 (square root of mass ratio of the gases).

As the gas permeation results could not unambiguously exclude the presence of connected meso-defects in the continuous membrane, permeation porometry measurements<sup>[32]</sup> were done for their quantitative assessment. Cyclohexane was used for selective blocking of intercrystalline pores below a certain size; simultaneous oxygen (kinetic  $\text{O}$  is 0.35 nm) permeation was used to determine the open porosity above that size.<sup>[28]</sup> Cyclohexane is too big to fit in the zeolite NaA micro-pores. Cumulative  $\text{O}_2$  permeance, measured during cyclohexane desorption, showed a primary inflection at  $\sim 20 \text{ nm}$  apparent  $\text{O}_p$ , creating an upper boundary for defect size detection (Fig. 9). Meso-defects  $>20 \text{ nm}$   $\text{O}_p$  could not be detected since they would be masked by the support. There was, however, no indication of any significant concentration of meso-defects  $<20 \text{ nm}$   $\text{O}_p$  in the membrane.

### 3. Conclusions

Highly oriented,  $1 \mu\text{m}$  thick zeolite A membranes have been grown repeatably by selective deposition of oriented seeds on a smooth macroporous  $\alpha\text{-Al}_2\text{O}_3$  support, followed by secondary growth. A significant negative surface charge density of the zeolites ensured suspension stability. A large,  $>180 \text{ mV}$ , difference in the related  $\zeta$  between A- and Y-crystals resulted in high selectivity for the sorption of the minority zeolite A phase onto a positively modified  $\alpha\text{-Al}_2\text{O}_3$  surface. Seed layer formation at proper zeolite suspension pH reproducibly resulted in a monolayer of pure, densely arranged, well-adhered, [200]-oriented zeolite A particles already after one adsorption cycle. A mixture of a weakly charged majority phase and a strongly charged minority phase led to an unusual

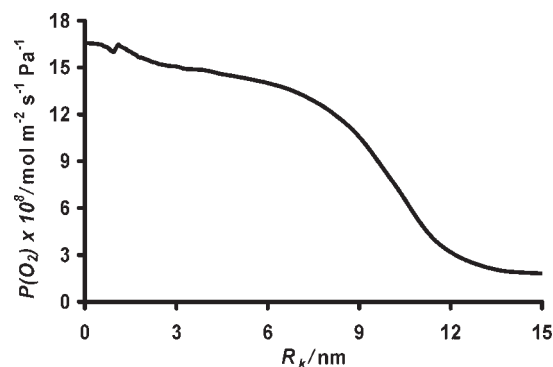


**Figure 9.** The cumulative  $\text{O}_2$  permeance as a function of Kelvin radius determined by permeation porometry.

dense packing of oriented zeolite A cubes. Subsequent multiple-layer deposition was hindered by the strong negative charge repulsion between the A monolayer and the dispersed particles.

Secondary crystal nucleation, and growth rates that are different in varying crystallographic directions of zeolite A phase, caused a gradual loss of orientation with secondary growth time. However, short-term epitaxial secondary growth led to a pure, continuous, [200]-oriented membrane as confirmed by electron microscopy, single gas permeation measurements and permeation porometry.

The results presented here for the preparation of continuous, thin, oriented zeolite membranes on macroporous supports are the first ever with this method. It can be expected that the selective adsorption technique shown will work for any mixture of strongly charged zeolite particles, present as a minority phase in a dispersion of particles with the same but weaker charge. The role of the majority phase is to prevent premature agglomeration, and to impede deposition of zeolite particles. This allows for the formation of a dense-packed structure during selective adsorption like the formation of large single crystals proceeds from a slightly supersaturated solution. Further improvements in membrane quality can be expected by obtaining narrower zeolite A and Y particle size distributions at optimum suspension concentration, and by using slower secondary nucleation rates to suppress the orientation losses.

### 4. Experimental

**Supports, Zeolite Dispersion, and Adsorption Procedure:** For the deposition experiments, we used  $\alpha\text{-Al}_2\text{O}_3$  disks with 2 mm thickness and 42 mm  $\text{O}$ , routinely produced in our group by colloidal processing of AKP15  $\alpha\text{-Al}_2\text{O}_3$  powder (Sumitomo Chemical Co. Ltd., Tokyo, Japan) followed by partial sintering [33]. These supports had a surface roughness (root mean square deviation from average) of  $\sim 25 \text{ nm}$ , a surface porosity (fraction of voids) of  $\sim 33\%$ , and a surface  $\text{O}_p$  of  $\sim 40 \text{ nm}$  [34].

Zeolite A seed layer was prepared by surface modification of the support with a cationic polymer [22–25], followed by selective adsorption from a suspension mixture of negatively charged zeolite

A and Y particles with optimized pH (see section “Zeta Potential Measurements and Zeolite A Seed Layer Formation” in Results and Discussion). PDDA (20 wt % solution in H<sub>2</sub>O,  $M_r = 100,000\text{--}200,000$ , Sigma-Aldrich, St. Louis, MO) and NaCl (99.6 wt % purity, Fischer Scientific, Fair Lawn, NJ) were used for initial support modification. A modification liquid was prepared by dissolving PDDA (50 mg of 20 wt % solution) in NaCl solution (50 ml of a 0.5 M solution in distilled water (Gradient A10 Milli-Q water distillator, Millipore, Billerica, MA)), and application of ultrasound for ~5 min to homogenize the mixture (FS30 ultrasonic bath, Fisher Scientific). The supports were immersed in the liquid with the deposition surface facing up for 20 min, followed by rinsing with distilled water to remove excess polymer and salt.

A powder mixture, synthesized by the method described in [26], of zeolite Y and 1 vol % A (estimated from XRD data by comparison of intensities of the  $2\theta = 6.19^\circ$  peak for zeolite Y and the  $2\theta = 7.20^\circ$  peak for zeolite A) was used for the seed layer adsorption step. The zeolite crystal suspension consisted of mixed powder (1 wt %) in distilled water at pH 11.7 (Orion 710Aplus pH/ISE meter, Richmond, VA) by adding tetramethylammonium hydroxide (TMAH, 10 wt % aqueous solution, prepared from 25 wt % aqueous solution, SACHEM, Austin, TX). Dispersing was enhanced by ultrasonic treatment for 4 h. During this treatment, the suspension temperature was kept below 23 °C by putting ice into the ultrasonic bath vessel.

The optimal pH for dispersed zeolite A and Y crystals was determined from zeta potential measurements by an electro-acoustic technique (ZetaProbe Analyzertm, Colloidal Dynamic Inc., Warwick, RI) at room temperature. The measurements were performed with commercially available 3  $\mu\text{m}$   $\varnothing$  zeolite 4A crystals (Wright Brothers, Cincinnati, OH) and 1  $\mu\text{m}$   $\varnothing$  zeolite Y crystals (Union Carbide, Danbury, CT). Both powders were dispersed in distilled water at a solid load of 1 wt %. After treating the suspensions with ultrasound for 15 min, the zeta potential was measured as a function of pH for each dispersion by titration with HNO<sub>3</sub> (1 M, EMD Chemicals, Gibbstown, NJ) to pH = 2.0 or TMAH (10 wt % aqueous solution) to pH = 12.5.

The zeolite adsorption experiments on PDDA-coated substrates were carried out by placing them horizontally, deposition surface up, into a zeolite sol for 80 min, followed by washing with distilled water. Polymer modification, zeolite adsorption, and related sample handling all took place in a clean-room environment with an air quality of better than class 1000 to reduce airborne contamination of the sample surface. Airborne contamination causes different types of defects which adversely affect membrane performance. After the adsorption procedure was complete, the supports were covered and dried at 40 °C in air for 24 h (Lindberg/Blue M oven, Asheville, NC). The organics were removed, and the zeolite/support adhesion was improved by calcination [27] in a programmed box furnace (Model 650-14, Fisher Scientific). The temperature program consisted of a maximum temperature of 400 °C for 3 h in air using a heating and cooling rate of 0.5 °C min<sup>-1</sup>.

**Membrane Secondary Growth:** Secondary growth was carried out in a capped polyethylene bottle at 80 °C in a Lindberg/Blue M oven. A homogenous synthesis solution with molar ratio composition of 10Na<sub>2</sub>O:1SiO<sub>2</sub>:0.02Al<sub>2</sub>O<sub>3</sub>:200H<sub>2</sub>O (NaOH pellets, Mallinckrodt, Hazelwood, MO; Na<sub>2</sub>Si<sub>3</sub>O<sub>7</sub> solution and NaAlO<sub>2</sub> powder, Sigma-Aldrich) was prepared based on the recipe of [35]. The seeded substrates were mounted horizontally, with the deposition surface down, to reduce adverse effects of material sedimentation from the bulk of the solution [9, 13, 15, 18]. For the same reason, the other, non-deposition side of the support was covered with a Teflon disk. The solution was then poured into the reactor until the membrane was fully immersed. The synthesis time was varied from 1 to 21 h. After quenching the reaction, supports were removed from the reactor, rinsed intensively with a spurt of warm distilled water, and dried in air at 40 °C for 24 h.

Since the films after the secondary hydrothermal step did not contain any organic template or additive, blocking the pore channels of the zeolite, a calcination procedure was not necessary.

**Sample Characterization:** The surface microstructure of the seeded supports, as well as the continuous membranes after secondary growth, was characterized by scanning electron microscopy with an XL-30 ESEM (Philips Electron Optics, Eindhoven, The Netherlands). Samples were mounted on an aluminium sample stub, covered with a carbon conducting tape, and coated with a 2–3 nm thick gold layer (Model 3 sputter coater 91 000 PELCO, Decatur, GA). The average  $\varnothing$  of the nano-zeolite particles in the seed layer was estimated by measuring the apparent dimensions of 30...50 distinguishable crystals, and was found to be 350–400 and 80–120 nm for zeolite A and Y, respectively.

The zeolite layer thickness was estimated from SEM of fracture cross-sections, and transmission electron microscopy of focused ion beam cross-sections (TEM: Philips CM200, 200 kV, Philips Electron Optics, Eindhoven, The Netherlands; FIB: DB235, FEI Corp., Hillsboro, OR). An element map of the sample cross-sections was obtained with an energy dispersive X-ray spectrometer, attached to the TEM, to clearly distinguish between the zeolite and alumina areas [21].

The phase purity and crystallinity of the initial zeolite powder, as well as the orientation of the seed layer and the continuous membranes were investigated by X-ray diffraction (XDS-2000, Scintag Inc., Cupertino, CA) using Cu K $\alpha$  radiation and a source operating at 45 kV and 20 mA.

**Gas Transport Measurements:** Steady-state single gas permeation measurements were conducted with different test gases (UHP grade He, H<sub>2</sub> and N<sub>2</sub> of 99.9% purity; Praxair Inc., Danbury, CT) to establish the presence of dominant microporous transport behavior. The measurements were performed at 170 °C with up to  $2 \times 10^5$  Pa pressure at the feed side, and vacuum (Triscroll 300 dry scroll pump, Varian, Palo Alto, CA) at the permeate side. The supported membrane was mounted inside a home-made permeation cell. This cell consists of two cylindrical stainless steel flanges with O-ring grooves and O-rings for gas-tight pressure sealing of the sample. The inlet and outlet of the cell were connected through stainless steel piping with a feed gas container and a vacuum pump, respectively. The absolute feed pressure was stepped up with a pressure transducer (870B Baratron<sup>®</sup>, 0–100 psia; MKS Instruments, Wilmington, MA), and the  $\Delta p$  across the membrane (independent variable) was measured with a differential pressure transducer (P55D, 0–80 psi range; Validyne Engineering, Northridge, CA). The gas permeance (dependent variable) was allowed to reach steady state for approximately 30 min at all pressures. The gas permeation flow was measured at the feed side with a mass flow meter (Brooks 5860E, 100 sccm full scale; Brooks Instruments, Hatfield, PA).

A custom built permeation porometry setup, described elsewhere [28, 32], was used to evaluate the presence of connected meso-defects in the continuous zeolite membrane. A desorption method was used, in which the membrane was first saturated for 48 h by allowing cyclohexane (99.9% purity, Fisher Scientific) to condense within it and close all active pores to gas permeation. After that, the cyclohexane vapor pressure was reduced gradually, allowing for the opening of pores with decreasing radii, and O<sub>2</sub> (UHP grade, Praxair Inc.) permeance was measured by monitoring its concentration in the permeate by gas chromatography (Varian CP-3800 GC, Varian).

Received: August 31, 2007

Revised: November 28, 2007

- [1] X. Gu, J. Dong, T. M. Nenoff, *Ind. Eng. Chem. Res.* **2005**, *44*, 937.
- [2] J. Hedlund, J. Sterte, M. Anthonis, A.-J. Bons, B. Carstensen, N. Corcoran, D. Cox, H. Deckman, W. D. Gijnst, P.-P. de Moor, F. Lai, J. McHenry, W. Mortier, J. Reinoso, J. Peters, *Microporous Mesoporous Mater.* **2002**, *52*, 179.

- [3] F. Bonhomme, M. E. Welk, T. M. Nenoff, *Microporous Mesoporous Mater.* **2003**, *66*, 181.
- [4] K. Kusakabe, T. Kuroda, A. Murata, S. Morooka, *Ind. Eng. Chem. Res.* **1997**, *36*, 649.
- [5] M. P. Bernal, E. Piera, J. Coronas, M. Menendez, J. Santamaria, *Catal. Today* **2000**, *56*, 221.
- [6] J. Sterte, S. Mintova, G. Zhang, B. J. Schoeman, *Zeolites* **1997**, *18*, 387.
- [7] M. E. Davis, *Nature* **2002**, *417*, 813.
- [8] Y. Kim, H. Lee, P. K. Dutta, *Inorg. Chem.* **2003**, *42*, 4215.
- [9] L. C. Boudreau, J. A. Kuck, M. Tsapatsis, *J. Membr. Sci.* **1999**, *152*, 41.
- [10] J. Hedlund, F. Jareman, *Curr. Opin. Colloid Interface Sci.* **2005**, *10*, 226.
- [11] J. Hedlund, *J. Porous Mater.* **2000**, *7*, 455.
- [12] P. Frontera, F. Crea, F. Testa, R. Aiello, *J. Porous Mater.* **2007**, *14*, 325.
- [13] S. Mintova, J. Hedlund, V. Valtchev, B. J. Schoeman, J. Sterte, *J. Mater. Chem.* **1998**, *8*, 2217.
- [14] L. C. Boudreau, M. Tsapatsis, *Chem. Mater.* **1997**, *9*, 1705.
- [15] M. Lassinantti, J. Hedlund, J. Sterte, *Microporous Mesoporous Mater.* **2000**, *38*, 25.
- [16] J. Hedlund, B. Schoeman, J. Sterte, *Chem. Commun.* **1997**, 1193.
- [17] F.-Z. Zhang, M. Fuji, M. Takahashi, *J. Am. Ceram. Soc.* **2005**, *88*, 2307.
- [18] Z. Lai, G. Bonilla, I. Diaz, J. G. Nery, K. Sujaoti, M. A. Amat, E. Kokkoli, O. Terasaki, R. W. Thompson, M. Tsapatsis, D. G. Vlachos, *Science* **2003**, *300*, 456.
- [19] Z. Lai, M. Tsapatsis, J. P. Nicolich, *Adv. Funct. Mater.* **2004**, *14*, 716.
- [20] H. Verweij, *J. Mater. Sci.* **2003**, *38*, 4677.
- [21] B. Oonkhanond, M. E. Mullins, *J. Membr. Sci.* **2001**, *194*, 3.
- [22] Y. Wang, Y. Tang, X. Wang, W. Shan, C. Ke, Z. Gao, J. Hu, W. Yang, *J. Mater. Sci. Lett.* **2001**, *20*, 2091.
- [23] W. Yang, X. Wang, Y. Tang, Y. Wang, C. Ke, S. Fu, *J. Macromol. Sci. Pure Appl. Chem.* **2002**, *39*, 509.
- [24] S. Y. Choi, Y.-J. Lee, Y. S. Park, K. Ha, K. B. Yoon, *J. Am. Chem. Soc.* **2000**, *122*, 5201.
- [25] G. S. Lee, Y.-J. Lee, K. B. Yoon, *J. Am. Chem. Soc.* **2001**, *123*, 9769.
- [26] J. E. Otterstedt, J. Sterte, B. J. Schoeman, *International Patent WO 94/05597*, **1994**.
- [27] M. Pan, Y. S. Lin, *Microporous Mesoporous Mater.* **2001**, *43*, 319.
- [28] M. L. Mottern, K. Shqau, F. Zalar, H. Verweij, *J. Membr. Sci.*, in press.
- [29] K. B. Yoon, *Acc. Chem. Res.* **2007**, *40*, 29.
- [30] C. Leiggenger, G. Calzaferri, *Chem. Phys. Chem.* **2004**, *5*, 1593.
- [31] *Collection of Simulated XRD Powder Patterns for Zeolites*, 4th ed., (Eds: M. M. J. Treacy, J. B. Higgins), Elsevier, Amsterdam **2001**.
- [32] M. L. Mottern, K. Shqau, D. Yu, H. Verweij, in *Proc. of ICIM9* (Eds: R. Bredesen, H. Raeder), SINTEF, Blindern, Norway **2006**.
- [33] K. Shqau, M. L. Mottern, D. Yu, H. Verweij, *J. Am. Ceram. Soc.* **2006**, *89*, 1790.
- [34] M. L. Mottern, J. Y. Shi, K. Shqau, D. Yu, H. Verweij, in *Membranes: Manufacturing and Applications*, (Eds: N. N. Li, A. G. Fane, W. S. W. Ho, T. Matsuura), Wiley, New York in press.
- [35] T. Çetin, M. Tatler, A. Erdem-Senatalar, U. Demirler, M. Ürgen, *Microporous Mesoporous Mater.* **2001**, *47*, 1.